Pressure broadening of Rb D_1 and D_2 lines by ^{3}He, ^{4}He, N_2, and Xe: Line cores and near wings

M. V. Romalis,* E. Miron,† and G. D. Cates
Physics Department, Princeton University, Princeton, New Jersey 08544
(Received 11 June 1997)

We studied the line shape of Rb D_1 and D_2 resonance lines in the presence of 1–10 amg of several gases: ^{3}He, ^{4}He, N_2, and Xe. We found that the line cores are well described by the asymmetric line shape expected for a van der Waals interatomic potential. The width and shift of the lines is proportional to the density of the foreign gas with high degree of accuracy, while the asymmetry is independent of the density. The constants of proportionality for pressure broadening and shift were measured with much higher accuracy than in previous experiments. We also studied the density dependence of the oscillator strength of the transitions. [S1050-2947(97)03212-5]

PACS number(s): 32.70.Jz, 32.70.Cs, 34.20.−b

I. INTRODUCTION

The study of pressure broadening of atomic resonance lines by collisions with neutral atoms has a long history starting with the work of Michelson [1], who observed that the linewidth increases with pressure in a roughly linear fashion. Early theoretical work by Lorentz [2] and Weisskorf [3] predicted a Lorentzian shape for the line core, treating the broadening as an interruption of the radiation wave train by collisions with gas atoms. This approach is called the impact approximation. Later work by Lindholm [4] and Anderson [5] also predicted a shift of the line center and a dispersionlike asymmetry of the line core. The experimental measurements of the line cores were reviewed by Chen and Takeo [6], Lewis [7], and Allard and Kielkopf [8]. The widths and shifts of the alkali-metal spectral lines in the presence of noble and other chemically inert gases have been studied very extensively, with perturber gas pressures up to several tens of atmospheres. The accuracy of most measurements, however, is only 10–20 %.

Another important feature of the pressure broadening is the formation of satellite lines. This effect is most easily explained in the framework of the quasistatic approach, first developed by Kuhn [9]. It relates the line intensity to the dependence of the energy difference between the atomic levels involved in the transition on the distance between the colliding atoms. An extremum in the energy difference results in the formation of a satellite line. Quasistatic formalism can be applied most successfully to the far wings of the atomic lines. In a series of papers, Gallagher and co-workers used the measurements of the far wing profiles to extract the interatomic potentials for a number of alkali-metal–noble-gas pairs [10].

A unified quantum-mechanical theory for the line core and wings was developed by Szudy and Baylis using the Franck-Condon treatment [11]. It also predicted a specific line shape for the line core and the satellite lines for a given interatomic potential. For the line core, the lowest-order correction to the Lorentzian line shape is a dispersionlike asymmetry. The first quantitative observation of the asymmetry was reported by Walkup, Spielfiedel, and Pritchard [12] for Na resonance lines in the presence of about 10 torr of several noble gases. Higher-order corrections can also be calculated for a specific interatomic potential. They were calculated for a van der Waals potential in Ref. [13]. A recent review by Szudy and Baylis [14] summarizes quantitative experimental and theoretical results on the line shape for the cores and far wings of spectral lines, including satellite lines.

Here we present a measurement of line cores and near wings of Rb D_1 and D_2 lines in the presence of ^{3}He, ^{4}He, N_2, and Xe. Our measurements are done for perturber gas densities ranging from 1 to 10 amg. Compared with previously available data, our results on linewidths, line shifts, and asymmetries are much more accurate. We also report on the first quantitative study of the spectral line cores exhibiting deviations from the Lorentzian line shape beyond the first-order dispersion asymmetry. Our results for the line shape are in good agreement with calculations of Ref. [13] for a van der Waals potential. We also present measurements of the pressure dependence of the D_1 and D_2 oscillator strengths.

One of the initial motivations for this work was an accurate determination of broadening and shift density coefficients, which then can be used to measure gas density in experiments using optical pumping. The technique of Rb optical pumping and spin exchange [15] finds many applications. ^{3}He polarized by this technique is used in measurements of the neutron spin structure functions [16], tests of fundamental symmetries [17], neutron polarizers and analyzers [18], and magnetic resonance imaging (MRI) of the lungs [19]. ^{129}Xe polarized by Rb-Xe spin exchange is used in MRI [20], surface studies [21], cross-polarization experiments [22], and other applications. N_2 and sometimes ^{4}He [23] are added to aid in the process of optical pumping. In some of these applications it is important to know accurately the density of the gas in the optical pumping cell. For ex-

*Present address: Physics Department, University of Washington, Seattle, WA 98195.
†Permanent address: NRCN, P.O. Box 9001, Beer Sheva 84910, Israel.

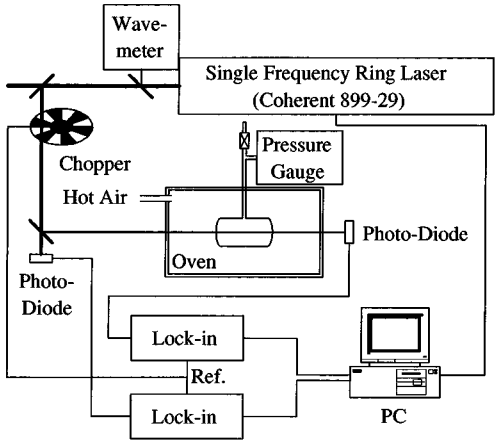

FIG. 1. Experimental setup. The laser intensity is attenuated by reflection from two optical blanks. The computer controlled the wavelength scan and stored the lock-in amplifier signals.

ample, in a recent precision measurement of the neutron spin structure function g_1^n at Stanford Linear Accelerator Center [16], the ^{3}He density in the target cells was determined with an accuracy of 1% by measuring the broadening and shift of Rb D_1 and D_2 lines, using the results of this paper as a calibration. Also, the knowledge of pressure broadening and the oscillator strength can be used to determine the Rb number density and for modeling the optical pumping process. These techniques were used in several experiments [24,25]. The choice of the gases used for this study, while motivated by the optical pumping experiments, provides a good sampling of noble (He is least polarizable, Xe is most polarizable) and diatomic (N_2) gases.

In Sec. II we describe our experiment, which uses a laser absorption method to measure the line profile. Section III describes the analysis technique, which is based on the classical limit of the unified Franck-Condon theory [11] for a van der Waals interatomic potential [13]. In Sec. IV, we present our results for the linewidth, line shift, asymmetry, and oscillator strength.

II. EXPERIMENTAL TECHNIQUE

In this experiment we used laser absorption spectroscopy. We measured the transmission of a laser beam through a cell filled with Rb vapor, and the perturber gas as the frequency of the laser was scanned through the resonance. This technique is free from the optical attenuation effects which can cause distortions of the line core in measurements based on the detection of fluorescence light. It also allows simple measurements of the oscillator strength, provided that the Rb number density is known. A schematic of the experiment is shown in Fig. 1. We used a single-frequency Ti:sapphire ring laser (Coherent 899-29) to scan across the absorption lines. The laser wavelength jitter was about 1 MHz, much smaller than the width of the pressure broadened lines, so no instrumental corrections were needed. The absolute wavelength was measured by a built-in wavemeter with an accuracy of 0.5 GHz, sufficient for shift measurements. The power of the laser was attenuated to a few mW/cm^2 by two reflections from uncoated glass to avoid saturating the atomic line. For this intensity the product of the optical excitation rate times the atomic lifetime $I\sigma\tau$ was always less than 3×10^{-4}. The laser beam was chopped at a frequency of 340 Hz. The incident and transmitted intensities were measured using silicon photodiodes. The signals were detected with lock-in amplifiers referenced to the chopper, and digitized by a computer. The same computer also controlled the wavelength scan. Fluctuations in the incident light intensity were canceled by dividing the transmitted intensity by the incident intensity. We also recorded the fluorescence coming from the cell. It was not used in the analysis of the line core because of significant optical attenuation, but was used to check the transmission measurements in the far wings. To check the linearity of the photodiodes and the absence of line saturation, we also performed measurements with the light intensity attenuated by a factor of 1000, to a few μW/cm^2. No changes in the line shapes were observed.

The cell used for the measurements was a simple cylinder 7.15 cm long. It was placed in a large oven heated by flowing hot air. The temperature was measured with a resistive temperature detector (RTD) and controlled by an analog Omega controller. We also measured the temperature with an accurate mercury thermometer. The air flow rate was stabilized using a pressure regulator. The temperature in the oven was stable to 0.1 °C with time and varied by less than 1 °C across the cell. For most measurements the temperature was 80 °C corresponding to Rb number density $[\mathrm{Rb}]=1.4\times10^{12}$ cm^{-3}, so the optical thickness on resonance varied between 0.3 and 5, depending on the density of the gas. Some measurements with ^{4}He were also done at 100 and 60 °C.

The signal to noise ratio was limited by two factors. The laser intensity fluctuations, which were on the order of 5–10 %, were not perfectly canceled by taking the ratio of the incident to transmitted intensity. In addition, because the coherence length of the laser is very long, the glass windows of the cell and the oven can act as etalons, resulting in oscillations of the transmitted intensity. This effect was reduced by expanding the laser beam. The signal to noise ratio is the worst for the highest density, because the optical thickness is small and the maximum absorption is only 30%. At low density, on the other hand, the absorption is very strong, and the line shape can be distorted by the finite dynamic range of the A/D board. The temperature and the length of the cell were chosen to find the best compromise between these two limitations.

The cell, made out of Pyrex, was initially baked under high vacuum, and a small amount of Rb was distilled into the cell. It was then filled with about 10 amg of the gas. About 8–12 measurements were performed with densities ranging from 10 to 1.5 amg. After each measurement some of the gas was released from the cell. When the pressure in the cell approached atmospheric pressure, the measurements were stopped. The cell was attached to the vacuum system, evacuated and filled with the next gas.

III. DATA ANALYSIS

The collision-broadened line profile is usually expressed in terms of the Fourier transform of the dipole autocorrelation function $\Phi(\tau)=\exp[-ng(\tau)]$ [5,11,14]:

$$I(\omega)\propto\frac{1}{2\pi}\int_{-\infty}^{\infty}d\tau\, e^{-i(\omega-\omega_0)\tau-ng(\tau)}, \tag{1}$$

where $g(\tau)$ is given in the classical approximation by

$$g(\tau)=\langle 1-e^{i\int_0^\tau dt\ \omega(R(t))}\rangle, \tag{2}$$

and n is the density of the foreign gas perturbers. Here $\omega(R)=[V_e(R)-V_g(R)]/\hbar$, where $V_g(R)$ and $V_e(R)$ are the interatomic potentials for the ground and excited state, respectively. $R(t)$ describes the path of the perturbing atom in the center of mass frame during the collision. For straight trajectories $R(t)=\sqrt{b^2+v^2t^2}$. The average $\langle\cdots\rangle$ is over the impact parameter b and thermal velocity v.

Equation (1) can be simplified for low perturber density by performing two integrations by parts and expanding the exponent in powers of n [14,26,27]. The low-density approximation is justified if the time between collisions is much longer than the duration of the collisions. This condition is satisfied for most of our data. The specific limits of applicability will be discussed later. With this approximation we obtain [14]

$$I(\xi)\propto\frac{\Gamma(\xi)}{\xi^2+(\gamma/2)^2}, \tag{3}$$

where $\xi=\omega-\omega_0-\Delta$. Here γ is the full width and Δ is the shift of the Lorentzian line core. They are defined in terms of $g(\tau)$ by $\gamma/2-i\Delta=ng'(\infty)$, which predicts a linear dependence of the width and shift on the gas density.

The dependence of Γ on the detuning ξ is responsible for deviations from the Lorentzian shape. In terms of the function $g(\tau)$ it is given by [14]

$$\Gamma(\xi)=\int_{-\infty}^{\infty}d\tau\, e^{-i(\omega-\omega_0-\Delta)\tau}g''(\tau). \tag{4}$$

To calculate $\Gamma(\xi)$ one needs to assume a specific shape for the difference potential $\omega(R)$. The calculation for a van der Waals potential $\omega(R)=[V_e(R)-V_g(R)]/\hbar=-C_6/R^6$ has been done in Ref. [13], and will be used in our analysis. The authors converted Eq. (4) to the following form [5,26,27]:

$$\Gamma(\xi)=n\left\langle v\int_0^\infty 2\pi b\ db\left|\int_{-\infty}^{\infty}dt\ \omega[R(t)]\times\exp\left[i\left(\xi t-\int_{-\infty}^{t}\omega[R(t')]dt'\right)\right]\right|^2\right\rangle, \tag{5}$$

assuming straight classical trajectories for $R(t)$. The results of their calculation are parametrized in the following fashion:

$$\Gamma(\xi)=nv_{\rm th}8\pi R_{\rm th}^2 I(\xi T_d), \tag{6}$$

where $T_d=C_6^{1/5}v_{\rm th}^{-6/5}$ is the duration of the collision, $R_{\rm th}=T_d v_{\rm th}$ is the effective radius of the collisions, and $v_{\rm th}=\sqrt{2kT/\mu}$ is the most probable thermal velocity in the center-of-mass frame. $I(x)$ is a dimensionless function of a dimensionless parameter $x=\xi T_d$ that contains all numerical information. If C_6 is positive (the excited state is more attractive than the ground state), then $x<0$ corresponds to the quasistatic wing (classically allowed transitions) and $x>0$ to the antistatic wing (classically forbidden transitions). The low-density approximation, used in derivation of Eq. (3), can be quantitatively expressed as $T_d\gamma\ll 1$, since the time between collisions is on the order of $1/\gamma$.

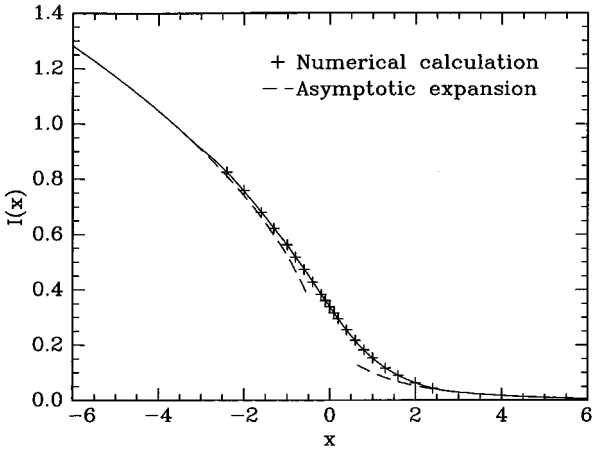

FIG. 2. Function $I(x)$ characterizing the deviation of the line shape from a Lorentzian profile calculated in Ref. [13] for a van der Waals potential. The dimensional parameter x is equal to the product of the frequency detuning $(\omega-\omega_0-\Delta)$ and the collision time T_d.

The function $I(x)$, calculated in Ref. [13], is plotted in Fig. 2. The calculation was done numerically for $-2.4<x<2.4$ with an accuracy better than 1%, except near $x=2.4$, where the error was $\leqslant 5\%$ [13]. For $x<-2.4$ the quasistatic result $I(x)=\pi/6\sqrt{x}$ is sufficiently accurate. For the antistatic wing $x>2.4$, one can use the result of an asymptotic expansion $I(x)=0.8464\sqrt{x}\,\exp(-2.1341\,x^{5/9})$ derived in Ref. [28]. We use a polynomial to interpolate between the calculated points, and smoothly match to the asymptotic functions. Near $x=0$, $I(x)$ is well approximated by a linear function $I(x)=0.3380-0.2245\,x$. It shows that the first-order correction to the Lorentzian profile is a dispersion term. This observation has been confirmed experimentally [12]. By making measurements at higher pressures (but still low enough for the low-density approximation to be valid), we can observe the nonlinear behavior of $I(x)$. We can also check the prediction of the theory that the asymmetry, parametrized by the collision time T_d, should be independent of the pressure.

The intensity transmitted through the cell I_T is given by

$$I_T=I_0\exp[-[\mathrm{Rb}]\sigma(\nu)L], \tag{7}$$

where I_0 is the incident intensity and L is the length of the cell. To extract the line profile from our data we plot $S(\nu)=\ln(G_T I_T/G_0 I_0)=-[\mathrm{Rb}]\sigma(\nu)L+\ln(G_T/G_0)$, where G_T and G_0 are the gains of circuits used to detect the transmitted and incident intensity, respectively. These data are fitted to the following equation:

$$S(\nu)=\frac{AI[2\pi T_d(\nu-\nu_c)]}{(\nu-\nu_c)^2+(\gamma/2)^2}+B, \tag{8}$$

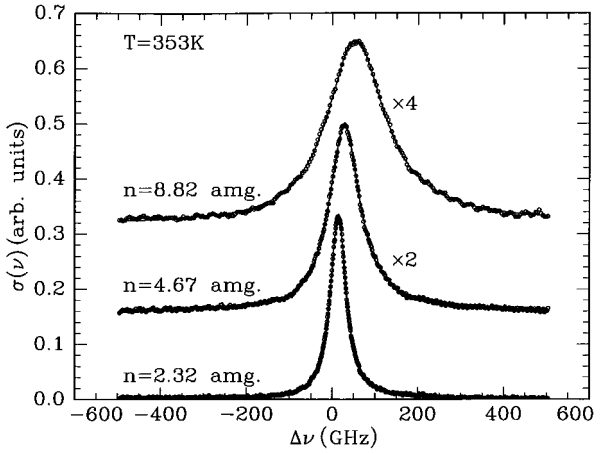

FIG. 3. Absorption cross section for a Rb D_1 line in the presence of three different densities of ^{3}He. The solid lines are fits to function (10). The curves have arbitrary offset and are scaled for better display.

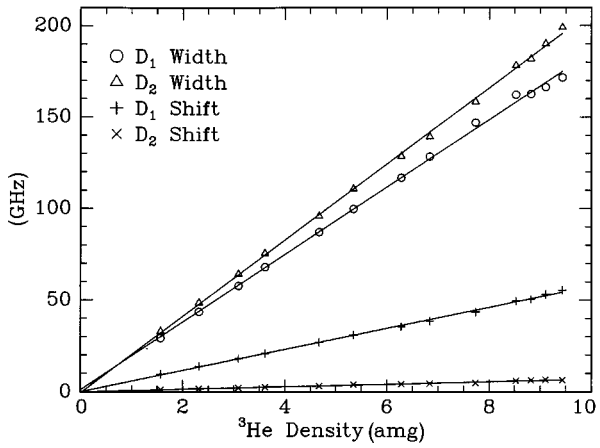

FIG. 4. The dependence of the shift and width of Rb D_1 and D_2 lines on the density of ^{3}He. The full width γ and shift Δ are determined from the fits of function (10) to the absorption cross sections.

where the constants A, B, T_d, ν_c, and γ are allowed to vary to minimize the χ^2 of the fit. The constant B absorbs the values of the instrumental gains, and does not carry any physical information. To correct for the ground state hyperfine splitting, we fit to the sum of four functions (two for each ^{85}Rb and ^{87}Rb) in form (8) with appropriate weights and shifts. This results in a very small correction. We ignore much smaller hyperfine splitting of the excited state. We also ignore Doppler broadening, which makes a negligible contribution to our width. The asymmetry due to collision correlations [29] is also negligible.

Also of interest is $\int \sigma(\nu) d\nu = \pi r_0 c f$, where $r_0 = 2.82 \times 10^{-13}$ cm is the classical electron radius and f is the transition oscillator strength. This gives us a relationship between the oscillator strength and the Rb number density. If we assume that the Rb number density is given by the equilibrium vapor pressure, we can measure the oscillator strength and study its dependence on the gas density.

We note that for a pure van der Waals potential the width, shift, and asymmetry can be calculated for a given value of C_6 [4]:

$$\gamma = 17.0 n v_{\mathrm{th}}^{3/5} C_6^{2/5},$$

$$\Delta = 0.182 \gamma, \tag{9}$$

$$T_d = C_6^{1/5} v_{\mathrm{th}}^{-6/5}.$$

However, these equations are not in good agreement with experimental data. Therefore, we vary all constants independently. Then we can compare our results with values predicted by Eqs. (9) using C_6 determined from measurements of the atomic polarizability [30].

IV. RESULTS AND DISCUSSION

A. ^{3}He and ^{4}He data

The D_1 absorption cross section for several pressures of ^{3}He is shown in Fig. 3. Because the value of the asymmetry is quite small, the results of the fit based on the Walkup function $I(x)$ are indistinguishable from the fit using only a first-order approximation, which gives a dispersionlike asymmetry

$$S(\nu) = \frac{A[1 + 0.664\ 2\pi T_d\ (\nu - \nu_c)]}{(\nu - \nu_c)^2 + (\gamma/2)^2} + B. \tag{10}$$

For example, for the largest value of T_d (D_1 line for ^{4}He), the detuning of 500 GHz corresponds to $x = 1$, the point where $I(x)$ just starts to deviate from the linear behavior. The dispersion form of the asymmetry can be derived without reference to a particular interatomic potential [31]. Our data agree very well with Eq. (10) for all densities studied. Small oscillations in the data for the highest density are due to the windows of the cell acting as etalons.

The dependence of the D_1 and D_2 linewidths and the shifts on the gas density is shown in Fig. 4. As predicted by the theory at low densities the dependence is quite linear. In all cases the offset of a linear fit is consistent with zero within error bars. The broadening and shift density coefficients are summarized in Table I. We also found that the asymmetry is independent of the density. Because the asymmetry is quite small, the best-fit value of the asymmetry is strongly correlated with the fit value of the line center. Therefore, in addition to fitting each pressure scan individually, we also fitted them simultaneously with a common value of T_d. When the number of adjustable constants is reduced from five per scan to about 4.1 (ten data sets are analyzed with a common value of T_d), the value of χ^2 increases by only 1–2 %. This confirms that the asymmetry is independent of the density.

The low-density approximation used in the analysis requires that $T_d \gamma \ll 1$. To check the validity of this approximation we calculate the critical density n_c for which $T_d \gamma = 1$. The most stringent constraint comes from the D_1 line in ^{4}He, which gives $n_c = 25$ amg. Thus the condition is satisfied, although not by a large margin. To check if the broadening and shift are slightly nonlinear due to the breakdown of the low-density approximation, we fit the lowest four data points independently. The broadening and shift coefficients change

TABLE I. Pressure broadening of Rb D_1 and D_2 lines by ^{3}He and ^{4}He. We give broadening and shift density coefficients and the degree of line asymmetry parametrized by the collision time T_d (independent of density). The last column gives the temperature dependence for the linewidth and line shift (see Fig. 5). This temperature dependence is used to scale the results of previous measurements to our temperature of 353 K. Negative values of T_d imply that $C_6<0$, i.e., the effective van der Waals difference potential is repulsive.

	^{4}He		^{3}He		Temp.
	This work	Previous results	This work	Previous results	depen.
D_1 full width (GHz/amg)	18.0±0.2	16.6±3 [32] 17.6 [33]	18.7±0.3	19.9±0.4 [35]	$T^{0.05\pm0.05}$
D_1 line shift (GHz/amg)	4.3±0.1	8.0 [34] 5.2 [33]	5.64±0.15	5.78±0.2 [35]	$T^{1.1\pm0.1}$
D_1 asymmetry, T_d (10^{-13}s)	−3.5±0.1		−1.9±0.1		
D_2 full width (GHz/amg)	18.1±0.2	17.4±3 [32] 19.4 [33]	20.8±0.2		$T^{0.53\pm0.06}$
D_2 line shift (GHz/amg)	0.46±0.06	0.77 [34] 1.8 [33]	0.68±0.05		$T^{1.6\pm0.4}$
D_2 asymmetry, T_d (10^{-13} s)	−0.44±0.1		−0.73±0.1		

by less than 1 σ. Therefore, we conclude that the low-density approximation remains valid for n/n_c approaching unity.

We have also studied the temperature dependence of the pressure broadening and shift. The temperature dependence can come from two effects. The average velocity of the collisions depends on temperature through $v_{\rm th}=\sqrt{2kT/\mu}$. In addition, the probability of finding a He atom a distance R from the Rb atom is proportional to $\exp[-V_g(R)/kT]$. However, if one assumes straight path trajectories for $R(t)$ in Eq. (2), this factor is neglected. Such an approximation is justified, because typical values of $V_g(R)$ for the line core correspond to about 5 K, much lower than the temperature of the atoms. Thus the factor $\exp[-V_g(R)/kT]$ is very close to unity. If all temperature dependence is due to the changes in the average velocity, then the data for ^{3}He are equivalent to the ^{4}He data taken at a temperature higher by a factor of $\mu_4/\mu_3=1.312$. Figure 5 shows the linewidths and line shifts for ^{4}He measured at 333, 353, and 373 K, as well as the data for ^{3}He taken at 353 K and converted to an effective ^{4}He temperature of 463 K. As can be seen, the scaling between the temperature and reduced mass is well satisfied. The temperature dependence is very different for the four quantities studied. This is to be contrasted with predictions based on the van der Waals R^{-6} interaction, which give a $T^{0.3}$ dependence for all four quantities [4]. We fit the temperature dependence to a power law T^n, with the results for n given in Table I.

This temperature dependence is used to convert previous measurements of the ^{4}He and ^{3}He width and shift density coefficients to our temperature. In general, our results are in agreement with previous measurements, although in some cases it is difficult to judge the agreement quantitatively because the authors do not quote a error for their data. There is only one measurement (^{3}He D_1 width and shift) with an accuracy comparable to ours [38]. Although the results for the shift are in good agreement, the width measurements disagree. This may be due to the fact that in [38] the authors use a different functional form to describe the line asymmetry, and do not correct for the broadening due to the laser spectral width of 18 GHz.

We can compare our results with predictions based on the

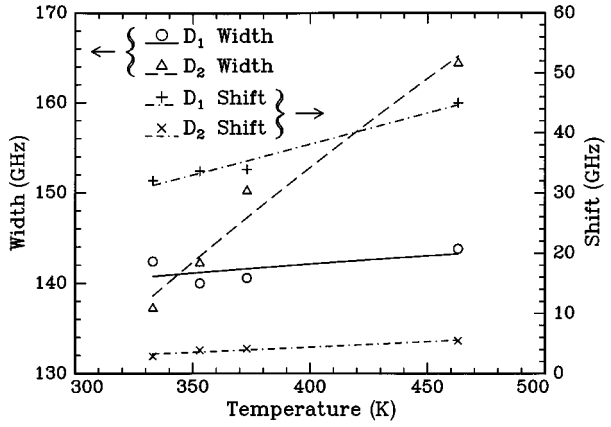

FIG. 5. The temperature dependence of the linewidth (plotted against the left axis) and line shift (plotted against the right axis) for He. The lowest three temperature points are for ^{4}He, while the highest point is for ^{3}He scaled as described in the text.

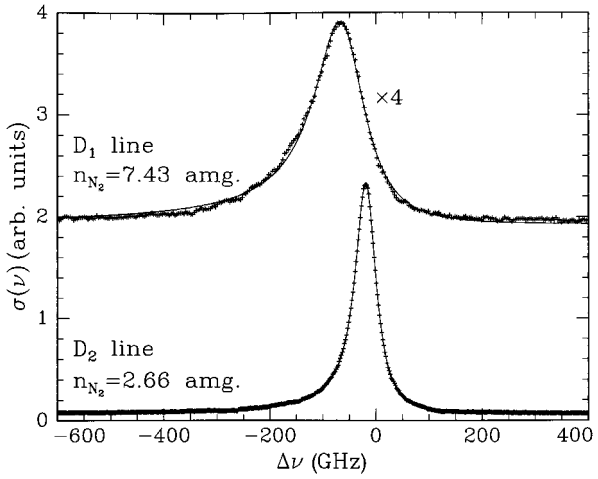

FIG. 6. The absorption cross-section for Rb D_1 and D_2 lines broadened by N_2, with fits to function (8).

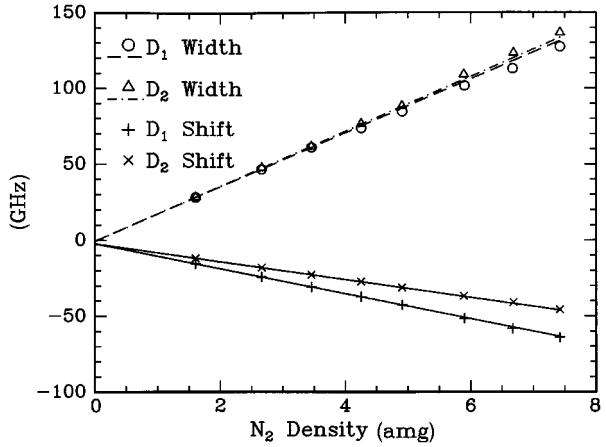

FIG. 7. Rb linewidths and line shifts as a function of N_2 density. The straight lines are fits to the lowest three data points, for which the low-density approximation is valid.

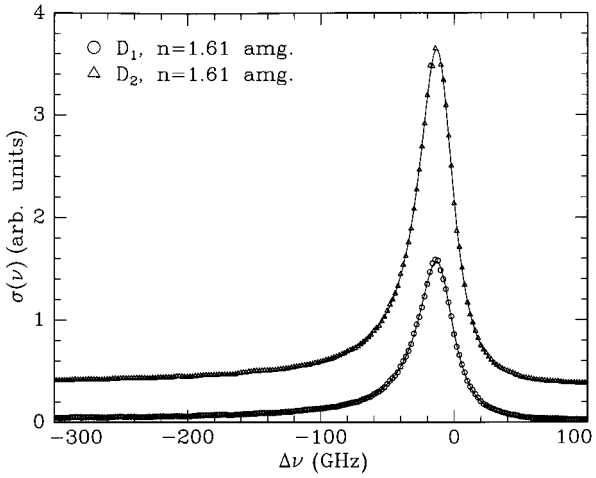

FIG. 8. Rb D_1 and D_2 lines in the presence of 1.61 amg of Xe with fits to function (8).

van der Waals interaction using Eqs. (9). The line center is shifted to the blue and $T_d<0$, which implies that the interatomic difference potential is repulsive (i.e., $C_6<0$). On the other hand, the long-range van der Waals interactions are always attractive, and larger for the excited state than for the ground state, so one expects $C_6=C_e-C_g>0$, as can be seen in Mahan's numbers derived from atomic polarizability [30]. However, because of the low polarizability of He, the Rb-He van der Waals interactions are very weak, and at shorter distances are overwhelmed by core repulsion [36]. Apparently, the line shift and asymmetry are dominated by the repulsive core interactions. The anomalously small value of the shift and asymmetry for the D_2 line is most likely due to cancelation of the effect of van der Waals attraction and core repulsion.

B. N_2 and Xe data

N_2 and Xe are heavier than He, and have a smaller thermal velocity. In addition, they are more polarizable and, therefore, have a stronger van der Waals interaction with Rb. As a result, the duration of the collisions $T_d=C_6^{1/5}v_{\rm th}^{-6/5}$ is longer and the low-density approximation is not satisfied for all densities studied. Figure 6 shows the absorption cross section for N_2 at two different densities. For N_2 the critical density corresponding to $T_d\gamma=1$ is equal to $n_c=5.5$ amg. As can be seen from Fig. 6, the line shape at the lower density ($n=2.66$ amg) is described very well by Eq. (8), while at $n=7.43$ amg it shows small systematic deviations. Figure 7 shows the values of the line shifts and linewidths as a function of N_2 density. As before, we find that the asymmetry is independent of density. To determine the pressure broadening and shift rates we fit only the lowest three data points with $n<4$ amg. For higher density the widths deviate slightly from the linear behavior, while the shifts remain quite linear. Table II summarizes our results for the density broadening and shift coefficients and the asymmetry. To our knowledge, no previous measurements for Rb-N_2 broadening exist. Because N_2 is diatomic, it has a large radiationless quenching and mixing cross sections, unlike the noble gases. This results in a reduction of the Rb excited-state lifetime, and contributes to broadening. Using the values of the cross sections from Ref. [37], we calculate that inelastic processes contribute 3.3 GHz/amg width to the D_1 line and 3.0 GHz/amg. to the D_2 line.

Figure 8 shows the absorption cross section for Xe with a

TABLE II. Broadening and shift density coefficients and line asymmetry for Rb D_1 and D_2 lines broadened by N_2 and Xe. Previous measurements for Xe are converted to our temperature of 353 K assuming $T^{0.3}$ temperature dependence for a pure van der Waals interaction. The last column shows the prediction for a van der Waals interaction for Xe calculated using Eqs. (9) and C_6 constants from Ref. [30].

	N_2	Xe		
	This work	This work	Previous results	van der Waals
D_1 full width (GHz/amg)	17.8±0.3	18.9±0.5	19.2±2 [32] 14.2 [38]	15.9
D_1 line shift (GHz/amg)	−8.25±0.15	−5.05±0.3	−6.95±0.7 [32] 6.5 [34]	−5.76
D_1 asymmetry, T_d (10^{-13} s)	16±2	35±2		34
D_2 full width (GHz/amg)	18.1±0.3	19.2±0.5	19.5 [32] 14.2 [38]	16.3
D_2 line shift (GHz/amg)	−5.9±0.1	−5.15±0.3	−8.34±0.6 [32]	−5.92
D_2 asymmetry, T_d (10^{-13} s)	12±1	35±2		34

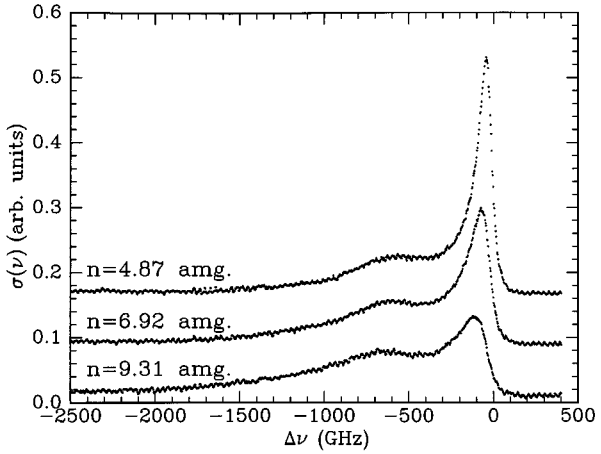

FIG. 9. Rb D_1 absorption cross section in the presence of high-density Xe.

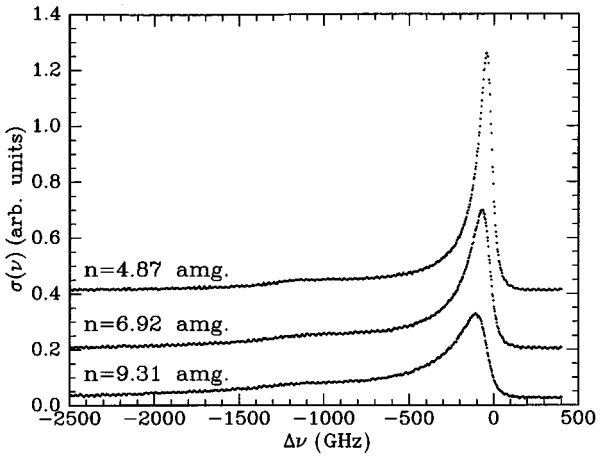

FIG. 10. Rb D_2 absorption cross section in the presence of high-density Xe.

fit to Eq. (8). The critical density for Xe is $n_c = 2.3$ amg. The line shape agrees very well with the data. The broadening and shift coefficients, given in Table II, are calculated from the data with $n < 2$ amg. The collision time T_d is independent of pressure within our error bars. Our numbers for the widths agree well with the results of Ottinger *et al.* [32], while our shift rates are substantially smaller. However, in Ref. [32] the shift is determined from the position of the line center at the half-height, which is affected by the asymmetry of the line. Table II also shows results predicted by Eqs. (9) for a van der Waals potential. We used $C_6 = 6.86 \times 10^{-58}$ erg cm^6 for the D_1 line, and $C_6 = 7.26 \times 10^{-58}$ erg cm^6 for the D_2 line from Ref. [30]. The agreement with experiment is reasonably good, especially for the collision time T_d.

Because the asymmetry is larger than for He, higher-order corrections to the line shape become important for Xe and N_2. For Xe, $2\pi T_d(\nu - \nu_c) = 1$ for detuning of 45 GHz, while for N_2 this happens at 100 GHz. To evaluate the importance of the higher-order effects, we tried to fit the data to the linear approximation (10) of the line shape. For both Xe and N_2 this resulted in an increase of χ^2 by a factor of 2–3. It is difficult to obtain a more significant confirmation of the higher-order effects in Eq. (8). For higher-order effects to be important, one would like to have $T_d \gamma \sim 1$. However, this is exactly the place where the low-density approximation starts to break down.

Equation (8) uses only one parameter (T_d) to characterize the asymmetry of the line. It is independent of the gas density, has a clear physical interpretation, and is in agreement with calculations. For comparison, we also tried to fit the data with several other functions which use two parameters to characterize the shape of the asymmetry that are free to vary with density. Nevertheless, we could not find a simple function which would consistently give a value of χ^2 better than or comparable to the results of Eq. (8). Therefore, we conclude that the function $I(x)$ calculated for a van der Waals potential in Ref. [13] is very successful in describing the shape of the line core, including corrections beyond the first-order dispersion asymmetry.

For Xe data with $n > 3$ amg, the line shape becomes significantly distorted by formation of a satellite line. Figures 9 and 10 show several absorption cross sections measured at densities ranging from 4.87 to 9.31 amg. The peak cross section of the line core goes down as $1/n$ with density, while the peak cross section of the satellite is proportional to n. Therefore, the relative size of the satellite line grows as n^2.

In the quasistatic theory of line shapes, the appearance of the satellite is associated with an extremum in the interatomic difference potential $\Delta V(R) = V_e(R) - V_g(R)$. If $d\Delta V(R_s)/dR_s = 0$, then a satellite line should appear at detuning $\nu_s = \Delta V(R_s)/h$. If the difference potential can be approximated by a parabola near the extremum, one can derive a characteristic line shape for the satellite [11]. However, we were not able to fit the data to such a line shape. We believe that for Xe-Rb the satellite is due to two extrema, one minimum and one maximum, located very close to each other. The Rb-Xe interatomic potentials relevant for the D_1 line are shown in Fig. 11 [10,39]. The difference potential has a minimum of 1544 GHz at $R = 5.77$ Å, and a maximum of 2042 GHz at $R = 7.06$ Å, while we observed the satellite at about 700 GHz. However, the shape of the interatomic difference potential near the extrema is very sensitive to the shape of $V_e(R)$ and $V_g(R)$. For example, if for the interatomic potential of the ground state we use the semiempirical

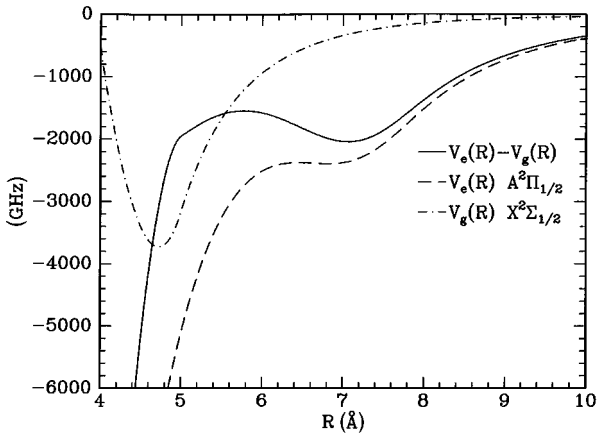

FIG. 11. Rb-Xe interatomic potentials for Rb ground state (dash dotted line) and the $P_{1/2}$ state (dashed line) taken from Refs. [10,39]. The solid line shows the difference potential, whose extrema are responsible for the formation of the satellite line.

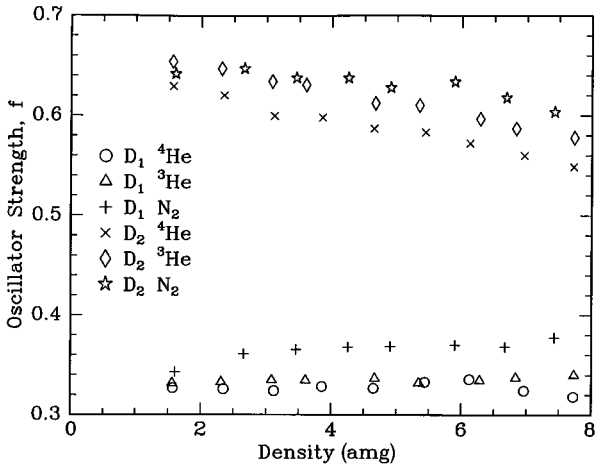

FIG. 12. The oscillator strength of Rb D_1 and D_2 lines determined from the integral of the absorption cross section a function of the gas density for ^{3}He, ^{4}He, and N_2.

calculation by Patil [40], the difference potential would have a minimum of 310 GHz at $R=5.88$ Å and a maximum of 1335 GHz at $R=7.29$ Å. The values of the maximum and minimum of the difference potential can probably be moved to 700 GHz by adjustments of the parameters which are consistent with other data from which the interatomic potentials where determined. Therefore, the position of the satellite can be used in combination with other data to determine more accurately the interatomic potentials. Once the interatomic potentials are determined, the shape of the satellite line can be used as a good test case to compare against the predictions of the unified satellite line-shape theory [11].

C. Oscillator strength

By integrating the absorption cross section over the wavelength, we can also obtain information on the oscillator strengths of the D_1 and D_2 transitions and their pressure dependence. This requires a knowledge of the Rb number density, which we can only determine from the vapor pressure curves. The cell was kept at 80 °C for a period of several days prior to each set of measurements, and the temperature was very uniform across the cell. Thus, it is reasonable to assume that the Rb vapor pressure should be close to equilibrium. To calculate the Rb number density we use data from Ref. [41], which have a quoted accuracy of 5%:

$$[\mathrm{Rb}]=10^{26.178-4040/T}/T. \tag{11}$$

At 353 K, this gives a density 7% higher than the more commonly used Killian formula [42]. However, Killian did not quote a error for his data.

Our results for the oscillator strength are shown in Fig. 12. The area is calculated from the parameters of the fit. This takes into account the area under the wings outside our measured range, which is on the order of several percent. It should be accurate for He because the low-density approximation is satisfied for all of our data, and the line shape agrees with data quite well. In addition, there are no significant satellite lines for He [32]. For N_2 our fits do not work very well at high pressures, so the numbers should be treated with caution. However, as can be seen in Fig. 12, the results for N_2 are similar to ^{3}He and ^{4}He. The uncertainty in the temperature of the cell is 0.5 °C, corresponding to a density error of 4%. The error in the length of the cell is 2%, and the error in the determination of the area under the absorption curve for ^{3}He and ^{4}He is 3%. The total error for our values of f is 7%, including the uncertainty in the vapor pressure curve.

We parametrize the density dependence of the oscillator strength by $f(n)=f\,(1+an)$. Because of the uncertainty in the estimation of the area for N_2 based on the fit, only ^{3}He and ^{4}He data are used for quantitative analysis. We find that the oscillator strength of the D_1 line is independent of pressure within our sensitivity: $|a_1|<0.003$ amg^{-1} (1σ), while the D_2 oscillator strength decreases with pressure: $a_2=-0.019\pm0.003$ amg^{-1} (the results for ^{3}He and ^{4}He are the same within errors). Our results for the oscillator strengths at zero pressure $f_1=0.33\pm0.02$ and $f_2=0.66\pm0.05$ are in very good agreement with commonly accepted values $f_1=0.322$ and $f_2=0.675$ [43]. We can compare our numbers with measurements by Chen [33], who studied the Rb oscillator strengths for ^{4}He densities up to 45 amg using a technique similar to ours. He found $a_1=-0.017$ amg^{-1} and $a_2=-0.019$ amg^{-1}. While the results for the D_2 line are in agreement, the pressure dependence of the D_1 oscillator strength is different from our result.

Since the sum rule $\Sigma f_i=1$ is almost saturated by the D_1 and D_2 transitions, $f_1+f_2=0.997$, their oscillator strength should decrease with density as the intensity of the forbidden transitions increases. The density dependence of the oscillator strengths for forbidden transitions has been studied in more details for Cs than for Rb [44–46]. The density dependence of the D_1 and D_2 transitions in Cs has also been studied in detail [47]. It was found that the ratio of the D_1 to D_2 oscillator strengths for Cs remains constant as the density is increased. This would imply that $a_1=a_2$ in agreement with Chen's Rb measurements [33]. On the other hand, it is difficult to find an effect which could systematically increase our values of the D_1 oscillator strength with density. If there is a significant area in the satellites which is not included in our integral, it would only result in the reduction of the apparent oscillator strength at higher densities. If the vapor pressure of Rb is reduced by the presence of He [48], it would also result in the apparent reduction of the oscillator strength with pressure. When the gas was released from the cell, some of the Rb vapor was released as well, temporarily reducing the Rb number density. This effect could result in the apparent reduction of the oscillator strength at low density. However, the vapor pressure comes back to equilibrium on a time scale given by the diffusion from the walls to the center of the cell, which is on the order of 6–30 s depending on the density. Each scan took about 5 min, and we alternated between first scanning the D_1 line followed by the D_2 line, and vice versa, after each release of the gas. Therefore, if this systematic effect were significant, it would have resulted in a systematic difference between odd and even points in our measurement, which was not observed.

V. CONCLUSION

We have reported a study of the line cores and near wings of the Rb D_1 and D_2 lines in the presence of 1–10 amg of

^{4}He, ^{3}He, Xe, and N_2. The measurements were performed using laser absorption spectroscopy, which is free from systematic effects that can cause distortions of the line shape. Unlike many earlier measurements, we extracted the values for the linewidth, line shift, and asymmetry by fitting the entire line shape with a theoretically well-motivated functional form. As a result, our parameters are measured in an unambiguous fashion without mutual correlation, and can be directly related to physical quantities. The accuracy of our data is in most cases significantly higher than in previous measurements. We have also confirmed with a high degree of accuracy that the linewidth and line shift increase linearly with density, and the line asymmetry, parametrized by the duration of the collisions, is independent of the density. These relationships are satisfied until the gas density becomes so high, that the time between collisions is comparable to the duration of the collisions.

We also studied the temperature dependence of the linewidth and line shift for ^{3}He and ^{4}He, and confirmed a scaling relationship between the temperature and reduced mass. Our line-shape data agree very well with calculations for a van der Waals potential made in Ref. [13]. By making measurements at densities comparable to the critical density, we have confirmed not only the first-order dispersion correction to the Lorentzian line shape, but also higher-order corrections. We have also obtained data for the Rb-Xe line shape at high Xe density exhibiting strong satellite lines, which can be used with other available data for accurate calculations of the interatomic potentials. We measured the oscillator strength of Rb resonance lines as a function of the foreign gas density, and observed a reduction of the oscillator strength for the D_2 line with density, but not for the D_1 line. Our data provide important tests of the pressure broadening theory and also will be useful in applications of optical pumping.

ACKNOWLEDGMENTS

We would like to thank Professor William Happer for stimulating discussions. This work was supported by U.S. DOE Contract No. DE-FG02-90ER40557 and NSF Contract No. NSF-9413901.

[1] A. A. Michelson, Astrophys. J. **2**, 251 (1895).
[2] H. A. Lorentz, K. Acad. Wet. (Amsterdam) **8**, 591 (1906).
[3] V. Weisskorf, Z. Phys. **77**, 398 (1932).
[4] E. Lindholm, Ark. Fys. A **32**, 17,1 (1945).
[5] P. W. Anderson, Phys. Rev. **86**, 809 (1952); P. W. Anderson and J. D. Talman, Bell Telephone Systems Report No. 3117, 1956 (unpublished).
[6] S. Chen and M. Takeo, Rev. Mod. Phys. **29**, 20 (1957).
[7] E. L. Lewis, Phys. Rep. **58**, 1 (1980).
[8] N. Allard and J. Kielkopf, Rev. Mod. Phys. **54**, 1103 (1982).
[9] H. G. Kuhn, Philos. Mag. **18**, 987 (1934).
[10] R. Hedges, D. Drummond, and A. Gallagher, Phys. Rev. A **6**, 1519 (1972); R. Scheps, C. Ottinger, G. York, and, A. Gallagher, J. Chem. Phys. **63**, 2581 (1975); G. York, R. Scheps, and A. Gallagher, *ibid.* **63**, 1052 (1975).
[11] J. Szudy and W. E. Baylis, J. Quant. Spectrosc. Radiat. Transf. **15**, 641 (1975).
[12] R. E. Walkup, A. Spielfiedel, and D. E. Pritchard, Phys. Rev. Lett. **45**, 986 (1980).
[13] R. Walkup, B. Stewart, and D. E. Pritchard, Phys. Rev. A **29**, 169 (1984).
[14] J. Szudy and W. E. Baylis, Phys. Rep. **266**, 127 (1996).
[15] T. G. Walker, and W. Happer, Rev. Mod. Phys. **69**, 629 (1997).
[16] K. Abe *et al.*, Phys. Rev. Lett. **79**, 26 (1997); Phys. Lett. B **404**, 377 (19977).
[17] R. E. Stoner, M. A. Rosenberry, J. T. Wright, T. E. Chupp, E. R. Oteiza, and R. L. Walsworth, Phys. Rev. Lett. **77**, 3971 (1996).
[18] G. L. Greene, A. K. Thompson, and M. S. Dewey, Nucl. Instrum. Methods Phys. Res. A **356**, 177 (1995).
[19] H. Middleton *et al.*, Magn. Reson. Med. **33**, 271 (1995).
[20] M. S. Albert, G. D. Cates, B. Driehuys, W. Happer, C. S. Springer, Jr., B. Saam, and A. Wishnia, Nature (London) **370**, 199 (1994).
[21] B. Driehuys, G. D. Cates, and W. Happer, Phys. Rev. Lett. **74**, 4943 (1995).
[22] B. Driehuys, G. D. Cates, W. Happer, H. Mabuchi, B. Saam, M. S. Albert, and A. Wishnia, Phys. Lett. A **184**, 88 (1993); G. Navon, Y.-Q. Song, T. R$\tilde{\text{o}}\tilde{\text{o}}$m, S. Appelt, R. E. Taylor, and A. Pines, Science **271**, 1848 (1996).
[23] B. Driehuys, G. D. Cates, E. Miron, K. Sauer, D. K. Walter, and W. Happer, Appl. Phys. Lett. **69**, 1668 (1996).
[24] P. Bogorad *et al.*, Nucl. Instrum. Methods Phys. Res. Sect. A (to be published).
[25] A. Baranga, S. Appelt, M. V. Romalis, C. J. Erickson, A. R. Young, G. D. Cates, and W. Happer, Phys. Rev. Lett. (to be published).
[26] V. I. Kogan and V. S. Lisitsa, J. Quant. Spectrosc. Radiat. Transf. **12**, 881 (1972).
[27] V. V. Yakimets, Zh. Éksp. Teor. Fiz. **51**, 1469 (1966) [Sov. Phys. JETP **24**, 990 (1967)].
[28] R. E. Walkup, Phys. Rev. A **25**, 596 (1982).
[29] I. Shannon, M. Harris, D. R. McHugh, and E. L. Lewis, J. Phys. B **19**, 1409 (1986).
[30] G. D. Mahan, J. Chem. Phys. **50**, 2755 (1969).
[31] J. Szudy and W. E. Baylis, J. Quant. Spectrosc. Radiat. Transf. **17**, 681 (1977).
[32] C. Ottinger, R. Scheps, G. W. York, and A. Gallagher, Phys. Rev. A **11**, 1815 (1975).
[33] S. Y. Chen, Phys. Rev. **58**, 1051 (1940).
[34] V. V. Gershun, V. Khutorschikov, and N. N. Yakobson, Opt. Spektrosk. **31**, 866 (1971) [Opt. Spectrosc. **31**, 470 (1971)].
[35] B. Larson, O. Häusser, P. P. J. Delheij, D. M. Whittal, and D. Thiessen, Phys. Rev. A **44**, 3108 (1991).
[36] J. Pascale, Phys. Rev. A **28**, 632 (1983).
[37] E. S. Hrycyshyn and L. Krause, Can. J. Phys. **48**, 2761 (1970).

[38] M. Takeo and S. Y. Chen, J. Quant. Spectrosc. Radiat. Transf. **4**, 471 (1964).
[39] R. J. Bieniek, Phys. Rev. A **15**, 1513 (1977).
[40] S. H. Patil, J. Chem. Phys. **94**, 8089 (1991).
[41] *CRC Handbook of Chemistry and Physics*, 74th ed. (CRC Press, Cleveland, 1993), pp. 4–124.
[42] T. J. Killian, Phys. Rev. **27**, 578 (1926).
[43] *Atomic, Molecular, and Optical Physics Handbook*, edited by G. Drake (AIP, New York, 1996).
[44] G. Moe, A. C. Tam, and W. Happer, Phys. Rev. A **14**, 349 (1976).
[45] B. Sayer, M. Ferray, and J. Lozingot, J. Phys. B **12**, 227 (1979).
[46] B. Sayer, M. Ferray, J. P. Visticot, and J. Lozingot, J. Phys. B **13**, 177 (1980).
[47] D. E. Gilbert and S. Y. Chen, Phys. Rev. **188**, 40 (1969).
[48] G. Wannier, *Statistical Physics* (Dover, New York, 1987), p. 372.